Generation and intensity-correlation measurements of the real Gaussian field

Cheng Xie, G. Klimeck, and D. S. Elliott
School of Electrical Engineering, Purdue University, West Lafayette, Indiana 47907
(Received 21 December 1989)

The generation of a broadband laser field with well-defined and controllable statistical properties, known as the real Gaussian laser field, has been achieved through the random modulation of the amplitude of a stabilized laser beam. The verification of the field-generation technique is provided by measurements of the laser power spectrum (Lorentzian) and by measurements of the intensity autocorrelation function. The latter is shown to decrease exponentially from an initial value of nearly 3 to a final value of 1 with a decay time related to the inverse bandwidth of the field. The techniques for generating this field and for its characterization are discussed in this paper.

INTRODUCTION

Laser bandwidth has been shown over the past several years to have a strong influence on qualitative and quantitative observations of multiphoton interactions. (See Refs. 1–6 for representative works in this area.) Calculations of these effects are typically based upon one of several different models of laser fields, and it has been established theoretically[1,7] that two lasers possessing the same power spectrum can produce significantly different results in nonlinear processes due to different higher-order statistical properties. Experimental verification of this has recently been provided in the microwave regime in comparisons of the phase diffusing field with the phase jump field.[8] In this report we discuss the laboratory generation of a field known as the real Gaussian field, and a study of its statistical properties. The ultimate goal of this project is the application of this field to nonlinear atomic systems for the direct comparison with the results of theoretical calculations[9] and with experimental results which test other field models.[10]

The real Gaussian field can be described by the expression

$$E(t)=E_0\varepsilon(t)e^{i\omega_L t}, \tag{1}$$

where $\varepsilon(t)$ is a fluctuating real amplitude and ω_L is a constant frequency. The random amplitude is a Gaussian process and the average value of $\varepsilon(t)$ is zero, i.e., it is positive as often as it is negative.

The method we use to generate this field involves the random amplitude modulation of the output of a stabilized dye laser using an acousto-optic modulator. This process has the ability to transfer the statistical properties of an rf drive voltage to the diffracted optical field. Generation of the optical real Gaussian field therefore depends upon our ability to generate an rf drive signal which has the properties of the real Gaussian field. This is done using a combination of rf mixers and hybrid junctions, as will be described later.

The real Gaussian field is closely related to the radiation field produced by a thermal source. (The latter has been referred to often as the chaotic field, a name which we will avoid here because of the recent explosion of interest in the chaotic behavior of nonlinear systems. We will instead use the name thermal field.) The real Gaussian field and the thermal field are similar in that each is characterized by strong intensity fluctuations. An important distinction, however, lies in the phases of the two fields. The field produced by a blackbody emitter is the superposition of fields of a large number of independent randomly phased elements of the source. As a result the phase of the resultant field is randomly distributed, and the field can be described as a complex variable

$$E(t)=E_0[\varepsilon'(t)+i\varepsilon''(t)]e^{i\omega_L t}, \tag{2}$$

where the two amplitudes $\varepsilon'(t)$ and $\varepsilon''(t)$ are real Gaussian variables with zero mean. In addition to a blackbody emitter, other sources of the thermal field include a laser operating on several independent, randomly phased longitudinal modes,[4] and light incident upon an ensemble of randomly distributed scatterers, such as a rotating piece of ground glass.[11]

The intensity fluctuations of the real Gaussian field are much stronger than those of the thermal field, as we will discuss in a later section. Larger intensity fluctuations are expected to lead to stronger laser bandwidth effects on nonlinear processes. For example, the two-photon absorption rate by a broadband absorber is expected to be enhanced by a factor of 3 for the real Gaussian field over that for a monochromatic field of the same average intensity, while the thermal field absorption rate is enhanced by a factor of only 2.[1] The frequency width of the two-photon absorption profile should be the same in each case, increasing as twice the laser width. In the case of the ac Stark effect associated with the saturation of a one-photon process, Georges[9] has calculated that the amplitude fluctuations of either field tend to wash out the Rabi sidebands as observed through resonance fluorescence measurements. Again this effect is more pronounced for the real Gaussian field.

Recently, Vemuri, Roy, and Agarwal[12] have developed a formalism to consider the effect on the resonance fluorescence spectrum when an atomic system is driven by a field which consists of a coherent and an incoherent

component. The incoherent component is modeled as the thermal field. Since the relative amplitudes of the coherent and incoherent parts are adjustable in their work, the authors are able to derive the change in the resonance fluorescence spectrum between the limits of monochromatic excitation and broadband excitation. This theory can be extended to the case where the incoherent part is the real Gaussian field,[13] which we are able to generate with our technique with a single adjustment within our electronics.

Recent interest[14,15] has also been directed towards the magnitude of the fluctuations of the fluorescence intensity scattered by an ensemble of atoms irradiated with a fluctuating field. The fluctuating field induces fluctuations in the fluorescence, potentially limiting the precision with which spectroscopic measurements can be made. The magnitude of these fluctuations is surprisingly large. Quantitative measurements of these effects, as induced by the phase-diffusion field, have recently been completed.[16] Calculations of the intensity fluctuations of the light transmitted by a Fabry-Perot interferometer have also been carried out.[17] These results are similar to the fluorescence intensity fluctuations except that the Fabry-Perot does not become nonlinear with increasing intensity.

The remainder of this paper is organized as follows. We first discuss in detail the technique we use of generating the real Gaussian field. We then present a description of some of the statistical properties of this field, as well as those of the thermal field, by way of comparison. A discussion of measurements of the power spectrum of the field, and of the intensity autocorrelation function appears last.

FIELD GENERATION TECHNIQUE

In order to generate the real Gaussian field, an acousto-optic modulator (AOM) is used to randomly amplitude modulate the output of a cw stabilized dye laser. The signal used to drive the acousto-optic modulator must therefore be randomly amplitude modulated as well. The AOM then transfers the randomly modulated amplitude to the diffracted laser beam.

The circuit used to modulate the amplitude of the drive signal is based upon an rf mixer, which can be used as a variable attenuator by applying a bias to the X port. Modulation of this bias signal results in modulation of the amplitude of the transmitted signal. This application of the mixer differs from the standard use of a mixer in which the L and R ports are used as input ports. We show in Fig. 1 that the transmission by the mixer from the L port to the R port is linearly dependent upon the bias voltage over a wide range of applied bias voltage. Bias voltages close to zero must be avoided where the transmission factor cannot be completely cancelled, as well as those for transmissions approaching unity where the response is nonlinear due to saturation. We have chosen an average bias voltage of about 1 V (see arrow in Fig. 1) and a maximum average amplitude (rms) of about 10 mV so that modulation of the amplitude of the transmitted voltage is linear. The range indicated in Fig. 1 is actually ten times this rms value since these large fluctuations of the Gaussian voltage must lie within the linear regime of the mixer. The signal which we apply to the X port of the mixer is of the form $V_m[a_0+\varepsilon(t)]$, where $V_m a_0$ and $V_m \varepsilon(t)$ represent the dc and fluctuating components of the bias voltage, respectively. This leads to an amplitude modulated signal appearing in the R port of the mixer of the form

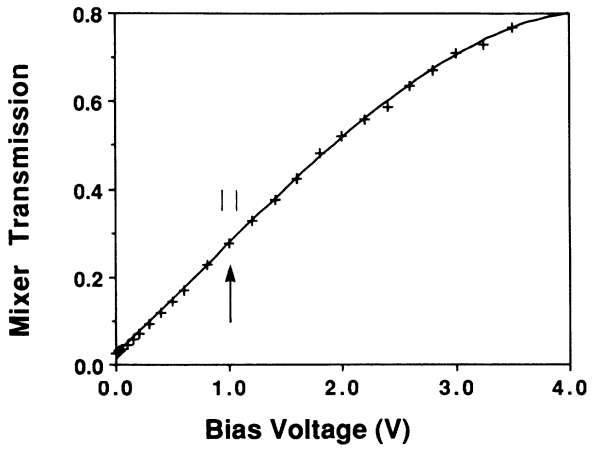

FIG. 1. The transfer function of the rf mixer used as a variable attenuator. The arrow indicates a typical dc bias level applied while the range of the fluctuating voltage (10 times the rms values) is shown by the pair of vertical bars.

$$V(t)=V_0[a_0+\varepsilon(t)]e^{i\omega_0 t}, \tag{3}$$

where the input to the mixer is at frequency $\omega_0/2\pi$ (200 MHz to match the drive requirements of our AOM). V_0 is the product of V_m, the slope of the mixer response (Fig. 1) and the amplitude of the 200-MHz input signal. As will be discussed in Sec. III, the spectrum of this signal, as observed on a spectrum analyzer, consists of a carrier (δ function) at frequency ω_0, and the spectrum of $\varepsilon(t)$ shifted up by the carrier frequency.

In order to represent the real Gaussian field, it is important to eliminate the carrier [i.e., the dc amplitude $V_0 a_0$ in Eq. (3)] from the signal generated by the technique described thus far. This is done by producing a second signal of the same frequency, phase, and average amplitude of the form $V_0 a_0 \exp(i\omega_0 t)$ and subtracting the two signals. A schematic of the rf circuit which accomplishes this cancellation is shown in Fig. 2. To ensure that the cancellation remains constant, a single source at frequency 200 MHz is used, and divided into two by a hybrid junction (HJ1). Half is directed to one mixer ($M1$) to produce the signal of Eq. (3). The other half is directed to a second mixer ($M2$) whose bias can be adjusted to precisely trim the amplitude to $V_0 a_0$. The two signals are subtracted in a second hybrid junction (HJ2) yielding a signal of the form

$$V(t)=V_0\varepsilon(t)e^{i\omega_0 t}. \tag{4}$$

Microstrip techniques are used throughout. The path lengths of the two lines between the hybrid junctions are

laid out to match the phase of the two signals as closely as is possible. Phase shifts which differ between the two halves of the circuit can still lead to incomplete cancellation of the carrier, however, and very fine tuning using a pair of high-Q adjustable capacitors ($\sim$5 pF) to ground at the input to each of the mixers is also required. Using this method, typical cancellation of the carrier to less than -90 dB m is attainable when -25 dB m total power is contained in the modulation signal. This translates into a ratio of the dc amplitude to the ac amplitude of Eq.

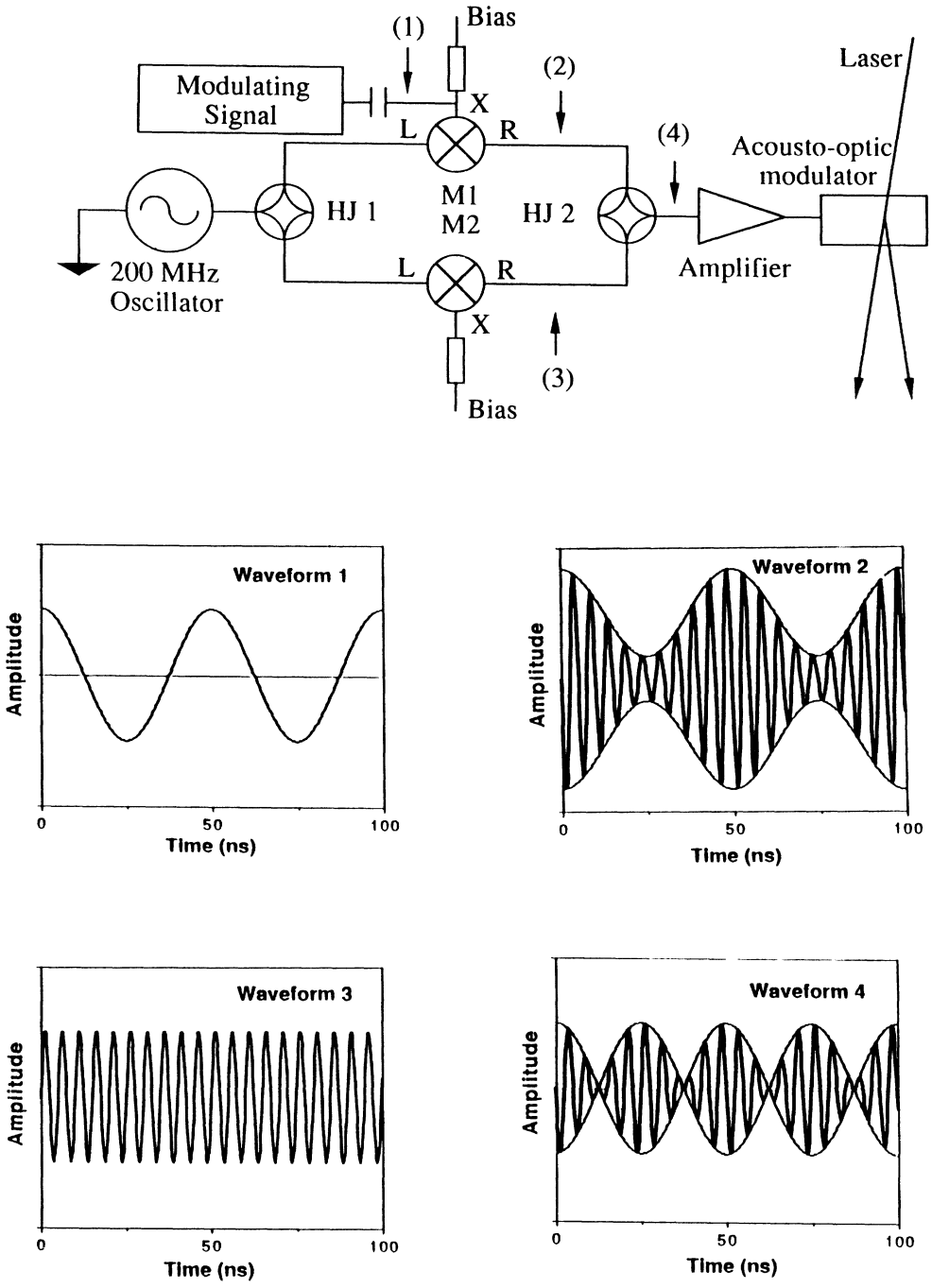

FIG. 2. Schematic of rf circuit which modulates the amplitude and suppresses the carrier of the AOM drive signal. The first hybrid junction (HJ1) splits the 200 MHz signal produced by the oscillator into two parts. Half is amplitude modulated by waveform 1 in mixer ($M1$) to produce waveform 2. The other half is attenuated in ($M2$) producing waveform 3. Hybrid junction (HJ2) subtracts these two waveforms to suppress the carrier, producing waveform 4.

(3) of about one part in 2000. Cancellation of the carrier is subject to drifts on a time scale of about 5 min, necessitating constant readjustment. The signal produced by this amplitude modulation circuit is amplified in a linear power amplifier which has a gain of 40 dB, an output power of 5 W, and a frequency range from 10–1000 MHz.

Generation of the modulation signal $V_m\varepsilon(t)$ is a very important aspect of this work as well, as the statistical properties of the real Gaussian field depend directly on the characteristics of $\varepsilon(t)$. The random noise signal is derived from a commercially obtainable noise source based on an avalanche noise diode. Pulses of electrons are generated through cascade collisions as they cross the p-n junction, following Poisson statistics which, in the limit of large average currents, approach Gaussian statistics. Extensive tests[18] on similar models of noise sources from the same manufacturer have been carried out to verify their statistical properties. We have not executed the same tests on these sources, but tests to be described later on the intensity correlations infer that the statistics of the noise sources are indeed very close to Gaussian. The noise source produces a flat spectrum from less than 50 kHz to greater than 1 GHz with a spectral density of -20 dB m/MHz. Frequencies greater than 80 MHz are filtered out in a pair of low-pass filters separated by coaxial attenuators.

The noise is next passed through an RC filter so that the power spectrum of the modulation signal assumes a Lorentzian shape:

$$S_m(\omega)=V_m^2 S_\varepsilon(\omega)\ , \tag{5}$$

where

$$S_\varepsilon(\omega)=\frac{S_0}{1+(\omega/\beta)^2}\ , \tag{6}$$

and $S_0=2\langle|\varepsilon(t)|^2\rangle/\beta$ represents the spectral density of the modulation signal at low frequencies ($\omega\ll\beta$). The correlation function of the fluctuation variable $\varepsilon(t)$ corresponding to his power spectrum can be easily obtained by the inverse Fourier transformation:[19]

$$R(\tau)=\langle\varepsilon(t+\tau)\varepsilon^*(t)\rangle=\langle|\varepsilon(t)|^2\rangle e^{-\beta|\tau|}\ . \tag{7}$$

We have constructed RC filters with the following half width at half maximum values $\beta/2\pi$: 0.80, 2.4, 4.5, 6.2, and 7.0 MHz. These filters are constructed on copper clad printed circuit boards using general purpose rf preamplifiers (10-dB gain, 50-Ω input-output impedance) as input and output buffers to eliminate reflections back to the noise source and reflections from the load. These amplifiers have low noise figure (<4 dB) and wide bandwidth (30 kHz–400 MHz). The filters produce spectra which are described by Eq. (6) to within 0.5 dB for all frequencies in the range 50 KHz–70 MHz. The saturation power level of the input and output buffers is $+15$ dB m, a minimum of 40 dB above the actual output power levels. Excess power capability of amplifiers and other rf devices must be available throughout the circuit to avoid clipping the voltage peaks, which would result in modification of the statistics of the noise. For example, if the saturation point of an amplifier is 13 dB higher than the average output power, the gain of the amplifier will be constant for voltage fluctuations as large as five times the rms value of the Gaussian voltage distribution. This excess gain factor is also important for the mixers and hybrid junctions in the amplitude modulation circuit, and for the power amplifier which drives the acousto-optic modulator. For these three components the excess power capabilities are a minimum of 38, 55, and 20 dB, respectively, so saturation is very effectively avoided here.

Saturation does become a problem, however, in the acousto-optic modulator. The acousto-optic modulator saturates at an input power close to one watt with a diffraction efficiency of about 60% at this power. We find that saturation effects start to become evident when the input power exceeds 15 dB m, as described later. At this power the diffraction efficiency is limited to about 4%. Since the optical power of the incident laser beam must be kept below 250 mW to avoid damage to the crystal, the power in the real Gaussian field is less than 10 mW. The transfer function of the AOM falls off by 3 dB at about 50 MHz to either side of the 200 MHz maximum response point.

An undesirable feature of the AOM is the dependence of the diffraction angle on the acoustic frequency. The diffraction angle in the acousto-optic crystal is given by λ/Λ_a, where λ is the optical wavelength in the crystal, and Λ_a is the wavelength of the acoustic wave. An amplitude-modulated signal therefore results in a spatially broadened laser beam, since the amplitude modulation power spectrum is spread in frequency about the carrier. The effect of this can be minimized, however, by using a lens to form the image of the diffracted beam in the interaction region where the effect of the real Gaussian beam is to be tested. In this way the Fourier components of the beam which exit the AOM at different angles are brought back together in the interaction region to reconstruct the whole beam.

Using the technique described in this section, we have achieved random amplitude modulation, with the carrier suppressed, of a stabilized laser beam. In the following section we will discuss the statistical properties of the real Gaussian field.

STATISTICAL PROPERTIES

We now turn our discussion to some of the statistical properties of the real Gaussian field. These are interesting because of their influence on nonlinear interactions, and their use in verification of the field-generation technique. In addition, this is a nontraditional field with unusual statistical properties and thus is interesting in its own right. Of particular importance to this work are the power spectra and correlation functions of the modulation signal, the rf drive signal, the laser field, and the laser intensity. The relationship between these various spectra, illustrated in Fig. 3, is discussed in this section, as well as the autocorrelation function of the intensity.

Because of the linear relationship between the modulating signal $V_m\varepsilon(t)$ and the amplitude of the rf drive signal (see Eq. 4), the power spectrum and correlation function given in Eqs. (6) and (7), respectively, apply to each

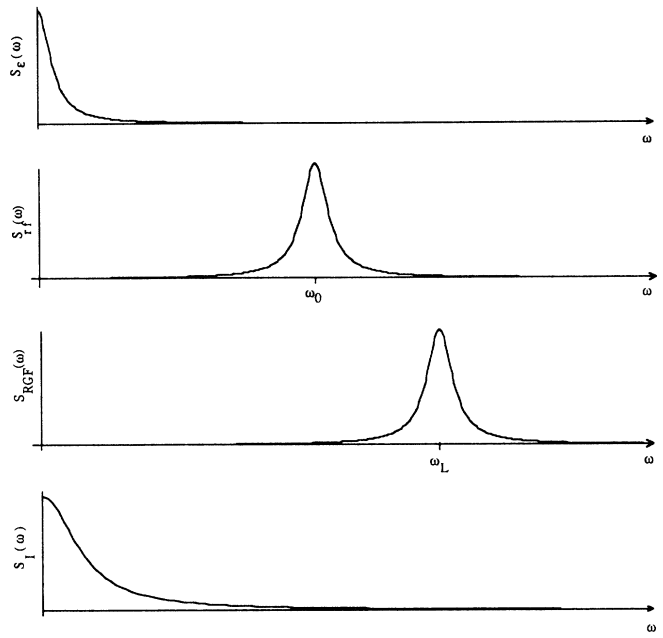

FIG. 3. Relationship between the power spectra of the modulation process. The plots show examples of the power spectra of the modulating signal $S_\varepsilon(\omega)$, the rf drive signal $S_{rf}(\omega)$, the optical signal $S_{RGF}(\omega)$, and the intensity fluctuations $S_I(\omega)$, respectively.

of these variables.

The power spectrum of the rf drive signal can be calculated from the autocorrelation function using Eq. (4).

$$\begin{aligned} S_{rf}(\omega) &= \int_{-\infty}^{\infty} \langle V(t+\tau)V^*(t)\rangle e^{-i\omega\tau} d\tau \\ &= V_0^2 \int_{-\infty}^{\infty} \langle \varepsilon(t+\tau)\varepsilon^*(t)\rangle e^{-i(\omega-\omega_0)\tau} d\tau \\ &= V_0^2 S_\varepsilon(\omega-\omega_0) \ . \end{aligned} \tag{8}$$

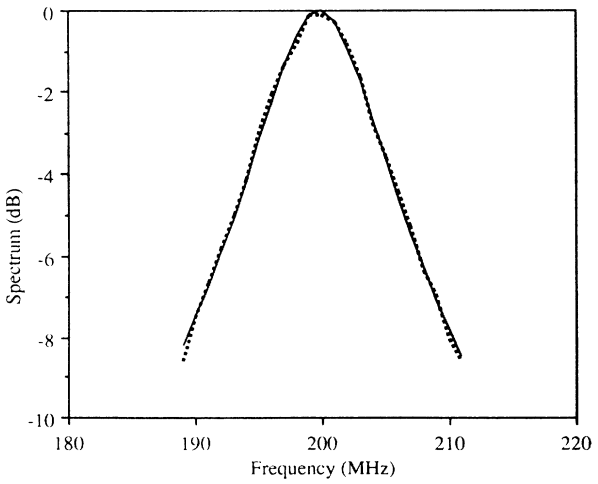

FIG. 4. Example of the power spectrum of the rf drive signal. The dashed line is the measured spectrum, the solid line is a fitted curve with width 4.5 MHz.

In other words, the spectrum of the rf drive signal is the same as the spectrum of the amplitude fluctuations, but shifted up in frequency by the carrier frequency ω_0. An example of the spectrum of the amplitude modulated rf drive signal is shown in Fig. 4.

The AOM is also a linear device, with the amplitude of the diffracted optical beam varying with the amplitude of the drive signal. Using the same logic as that used to derive Eq. (8), it is shown that the power spectrum of the real Gaussian field is given by

$$S_{RGF}(\omega) = E_0^2 S_\varepsilon(\omega-\omega_L) \ . \tag{9}$$

Measurement of the rf power spectrum is useful for monitoring the generation of the real Gaussian field. For instance, if the carrier is not suppressed sufficiently, the power spectrum has an extremely narrow band spike at the carrier frequency. In this case the amplitude has a nonzero dc component, as in Eq. (3). The spectral density of the laser is therefore

$$S_{rf}(\omega) = V_0^2[2\pi a_0^2 \delta(\omega-\omega_0) + S_\varepsilon(\omega-\omega_0)] \ . \tag{10}$$

The ratio of the average power in the carrier to that in the incoherent part of the spectrum is $a_0^2\langle|\varepsilon(t)|^2\rangle$. As we remarked in the preceding section, the carrier is typically suppressed to a power level 65 dB below the integrated incoherent power level, so that $a_0 \cong [\langle|\varepsilon(t)|^2\rangle]^{1/2}/2000$. This level of suppression is considered sufficient for all purposes for which this field is intended.

An additional test of the statistical properties of the field generated by this technique is afforded by measurement of the intensity autocorrelation function,

$$\begin{aligned} R_I(\tau) &= \frac{\langle I(t+\tau)I(t)\rangle}{\langle I(t)\rangle^2} \\ &= \frac{\langle E(t+\tau)E^*(t+\tau)E(t)E^*(t)\rangle}{\langle|E(t)|^2\rangle^2} \\ &= \frac{\langle \varepsilon(t+\tau)\varepsilon^*(t+\tau)\varepsilon(t)\varepsilon^*(t)\rangle}{\langle|\varepsilon(t)|^2\rangle^2} \ . \end{aligned} \tag{11}$$

Since the field amplitude is a Gaussian process, the fourth-order field correlation function can be written[19] as the sum of the product of all pairings of second-order correlation functions of the field

$$\begin{aligned} R_I(\tau) = [&\langle \varepsilon(t+\tau)\varepsilon^*(t+\tau)\rangle\langle \varepsilon(t)\varepsilon^*(t)\rangle \\ &+ \langle \varepsilon(t+\tau)\varepsilon(t)\rangle\langle \varepsilon^*(t+\tau)\varepsilon^*(t)\rangle \\ &+ \langle \varepsilon(t+\tau)\varepsilon^*(t)\rangle \\ &\times \langle \varepsilon^*(t+\tau)\varepsilon(t)\rangle]/\langle|\varepsilon(t)|^2\rangle^2 \ . \end{aligned} \tag{12}$$

The first of these terms is unity, since the numerator can be seen to be the square of the average intensity. Using Eq. (7), the second and third terms for the real Gaussian field each yield $(e^{-\beta|\tau|})^2$, leading to an auto-correlation function of the form

$$R_I(\tau) = 1 + 2e^{-2\beta|\tau|} \ . \tag{13}$$

This function decreases from a value of 3 to a value of 1

with a correlation time one-half that of the field correlation function.

It is interesting to compare the autocorrelation function of the real Gaussian field to that of the thermal field. When the amplitude is a complex variable such that the real and imaginary parts are statistically independent of each other and have the same correlation function, the second term in the expression for $R_I(\tau)$, Eq. (12), becomes zero. The thermal field satisfies these conditions, and thus its intensity autocorrelation function becomes

$$R_I(\tau)=1+e^{-2\beta|\tau|}\ , \tag{14}$$

having a maximum value of only 2. This comparison is the basis of the previous claims that the real Gaussian field was characterized by stronger fluctuations than the thermal field. The physical reason for this is based on the frequency of the occurrence of low instantaneous intensities for the two fields. The real Gaussian field has deep minima, since the field amplitude has zero as its most likely value. (It is a Gaussian distribution with a zero mean value.) The thermal field, on the other hand, seldom has a zero instantaneous intensity, since this requires that both quadratures of the amplitude be zero. The real Gaussian field therefore has deeper minima, leading to stronger intensity fluctuations.

Another illustration of how the deep minima of the instantaneous intensity can affect the intensity autocorrelation function can be found in the example of the incomplete suppression of the carrier. In this case the field amplitude becomes $a_0+\varepsilon(t)$ and the maximum value of the intensity autocorrelation function can be shown to be

$$R_I(0)=3-2[1+\langle|\varepsilon(t)|^2\rangle/|a_0^2|]^{-2}\ . \tag{15}$$

It can be seen that if the power in the carrier equals that of the incoherent part of the spectrum, the maximum value of the intensity autocorrelation function is reduced to a value of 2.5. In the coherent field limit $[\varepsilon(t)\ll a_0]$ this function reduces to 1, as expected. For the suppression of the carrier which we can typically attain, $R_I(0)$ is reduced by only 2×10^{-13}, a value which is completely unobservable. When suppression of the carrier is not so complete, however, measurement of $R_I(\tau)$ is sensitive to this factor.

Comparison of measurements of our field statistics with the properties of the real Gaussian field described in this section provides an important test of our field generation technique. In the final section of this paper, we discuss measurement of the statistical properties of the field generated with our technique, and compare the results of these measurements with those expected for the real Gaussian field.

CORRELATION MEASUREMENTS

We use two tests of the final laser field in order to demonstrate successful generation of the real Gaussian field. Of greatest concern is the prevention of residual phase shifts induced by any of the elements (they may or may not be correlated to the amplitude fluctuations), or saturation of the signal leading to clipping of the peak amplitudes.

The first test of the field is a measurement of the laser power spectrum, accomplished by either of two means. One method employs a scanning Fabry-Pérot interferometer, whose transmission as a function of cavity length yields the laser spectral density directly. The major disadvantage of the Fabry-Pérot interferometer for this application is one of alignment. Since the diffracted beam is spatially spread out due to the broadband drive signal, coupling into the cavity is not straightforward, and the measured spectrum of the laser is not without ambiguity. We have found heterodyne detection of the laser spectrum to be preferable because of these difficulties. In this case, the real Gaussian field and a monochromatic "local oscillator" are combined and focussed onto a photodiode. The local oscillator beam is produced by the same laser, and separated from the laser output before it passes through the AOM. It is therefore narrow band ($\sim$200 kHz), and differs in frequency from the real Gaussian field by 200 MHz. The current produced by the photodiode at the beat frequency can be spectrally analyzed to produce the spectrum of the modulated laser field. The power spectra of the heterodyne signals typically match the power spectra of the rf drive signal quite well close to line center, but drop off at frequencies farther away from line center due to the limited frequency response of the AOM. The symmetry of these curves again help verify the low level of any phase modulation which might be present. The heterodyne signal can also be displayed directly on an oscilloscope, an example of which is shown in Fig. 5. In this case, the laser was modulated with a single frequency signal at 5 MHz. The amplitude can clearly be seen to change sign every 100 nsec. The tic marks help guide the eye by marking every period of the 200-MHz carrier, initially lining up with the negative peaks, then the positive peaks, and finally the negative peaks again. No residual phase modulation is observable in the figure.

The second test of the field statistics is provided by

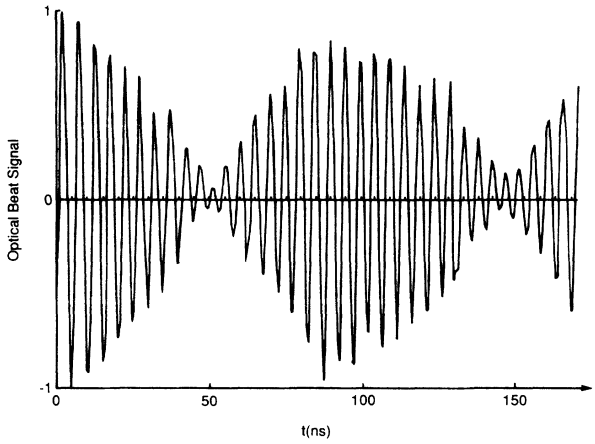

FIG. 5. Time-dependent signal produced by beating the single tone modulated (5 MHz) laser against a local oscillator field produced from the same laser source. The heterodyne frequency is 200 MHz.

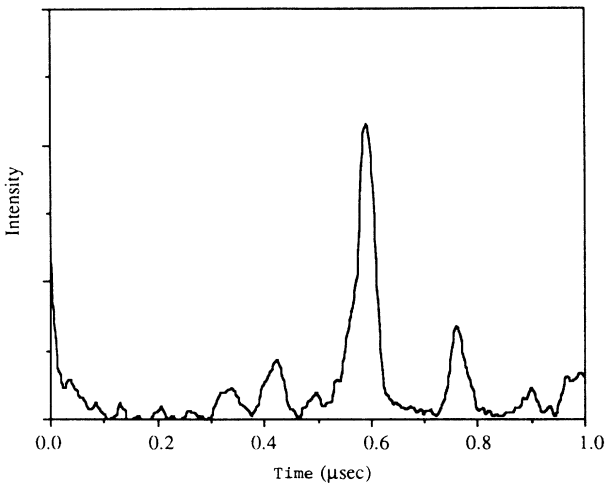

FIG. 6. Example of the time-varying intensity of the real Gaussian field.

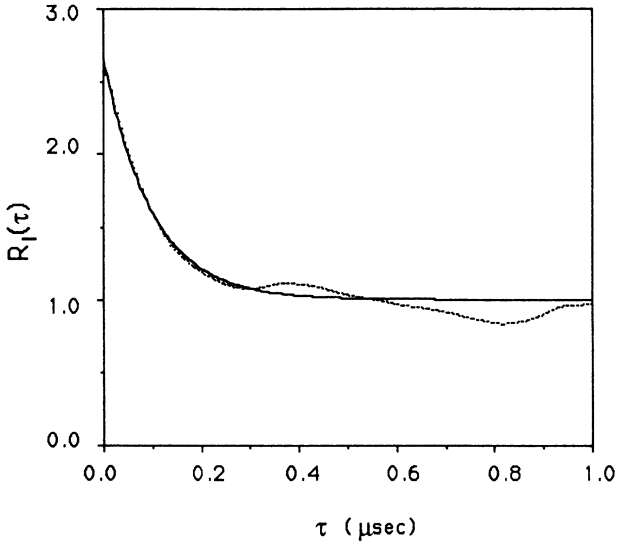

FIG. 7. Example of the autocorrelation function of the real Gaussian field. This data, shown by the dashed line, corresponds to $\beta/2\pi=0.8$ MHz. The solid line represents the best fit to the data.

measurement of the intensity autocorrelation function. To make this measurement, the broadened laser beam is directed onto a photodiode (no local oscillator beam is present). The photocurrent is thus proportional to the laser intensity integrated over the area of the photocathode. Figure 6 shows a typical oscilloscope trace of the intensity waveform when the laser amplitude is randomly modulated. Intensity waveforms are repeatedly digitized and stored using a charge-coupled-device (CCD) camera attachment to the oscilloscope interfaced to a laboratory computer. The CCD array has 490 (vertical) by 384 (horizontal) pixels, but the resolution is somewhat less than this due to the thickness of the oscilloscope trace. The intensity autocorrelation is computed from a compilation of 26 disjoint, digitized waveforms. The finite duration of each individual waveform limits the data set for calculation of $R_I(\tau)$ for large τ, so each waveform must be many correlation times $[(2\beta)^{-1}]$ long. Conversely, the intensity correlation time must be much larger than the resolution of the camera system so that the intensity fluctuations are not averaged away. By keeping within these confines, we have been able to measure the intensity autocorrelation function for each of the noise filters constructed, and a typical example is shown in Fig. 7. This data is for the 0.8-MHz filter, giving a 1.6-MHz laser width (full width at half maximum). The dotted line is the measured function, while the solid is a best fit approximation to the dotted line of the form

$$R_I(\tau)=1+[R_I(0)-1]e^{-\tau/\tau_C} . \tag{16}$$

Uncertainties in the measured function are typically ± 0.05 (1σ standard deviation) as determined from the scatter in the data. Ideally $R_I(0)$ should be 3, while the correlation time τ_C should be $(2\beta)^{-1}$. The fitted parameters $R_I(0)$ and τ_c, are given in Table I for the maximum

TABLE I. Summary of results. Maximum value of the autocorrelation function of the intensity and the correlation time for the five filters used. The fitted values of $R_I(0)$ and the correlation time, determined for only one data set for each filter, are those values which minimize the deviation of Eq. (16) from the data.

Filter width $\frac{\beta/2}{(\text{MHz})}$	$R_I(0)$		Correlation time (nsec)	
	Measured	Fitted	$(2\beta)^{-1}$	Fitted
0.8	2.57 2.65	2.68	99.0	97.2
2.4	2.64 2.57	2.81	33.0	32.7
4.5	2.58 2.61	2.74	17.0	13.9
6.2	2.46 2.47	2.56	12.8	11.0
7.0	2.24 2.27	2.38	11.3	13.4

amplitude fields we consider to be usable for our application. Larger amplitudes lead to saturation in the AOM and an associated decrease in $R_I(0)$. The measured values of $R_I(0)$ in Table I are obtained from the intensity correlation data such as that shown in Fig. 7.

The most significant factor in the deviation of $R_I(0)$ from 3 is, we believe, the averaging of the instantaneous intensity provided by the AOM, the photodetection, and the waveform digitizing system. The first of these is due to the finite velocity of the acoustic wave in the acousto-optic crystal and the nonzero size of focused laser beam in the crystal. This results in a variation of the acoustic wave amplitude from one side of the beam to the other. We can estimate the magnitude of this effect by calculating in one dimension, the time-averaged square of the beam power, normalized to the square of the average power,

$$\frac{\langle P^2\rangle}{\langle P\rangle^2}=\frac{\langle \int I(x')dx' \int I(x'')dx''\rangle}{\langle \int I(x')dx'\rangle^2}\ , \tag{17}$$

where x is the spatial variable in the direction of propagation of the acoustic wave, i.e., across the laser beam cross section. Exchanging the order of multiplication, integration, and time averaging in the numerator allows us to write the numerator of Eq. (17) in terms of the intensity autocorrelation function given by Eq. (13). Evaluating this expression for the case of a square profile of the laser beam intensity yields an averaged square power

$$\frac{\langle P^2\rangle}{\langle P\rangle^2}=1+\frac{2}{\beta T}+(\beta T)^{-2}(e^{-2\beta T}-1)\ , \tag{18}$$

where T is the transit time of the acoustic wave across the laser beam waist. We estimate the transit time as $\sqrt{\pi/2}\,w_0/v_a$ where w_0 is the beam radius (e^{-2} intensity point) and v_a is the acoustic velocity in the crystal. For our geometry $w_0=60$ μm, and $v_a=4.26$ μm/nsec for the AOM crystal (TeO_2), yielding an estimated transit time of 18 nsec. Equation (18) is shown as the solid line in Fig. 8. The data points represent the measured values of the $R_I(0)$ for the five filters. The estimate of this effect is certainly not expected to be precise, as we have not accounted for the Gaussian beam profile. It does appear however that signal averaging in the AOM, as estimated here, and in the detection system, is sufficient to account for the deviation of $R_I(0)$ from 3. We also remark that this factor may have only a minimal effect when this field is applied to an atomic vapor for testing of the laser bandwidth effects. The atom will not be responsive to the variation in intensity across the beam but rather to the local intensity and its temporal coherence. For this reason we believe this factor will not seriously affect our ability to apply this field to nonlinear interactions.

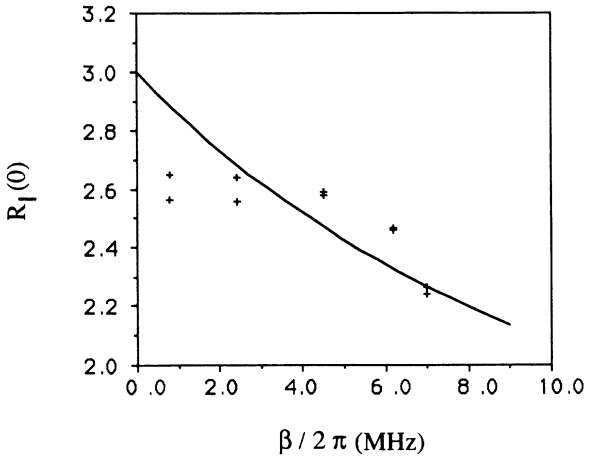

FIG. 8. $R_I(0)$ vs $\beta/2\pi$ for the five filters. The data points are the results of the measurements computed from the time-dependent intensity waveforms. The solid line is the function given by Eq. (18).

CONCLUSION

Generation of the real Gaussian field will now allow laboratory testing of laser bandwidth effects in a variety of nonlinear optical interactions. Measurements performed on this field have confirmed the unique properties of the real Gaussian field. Two tests of laser bandwidth effects are now being set up. The first is Doppler-free two-photon absorption, where it will be of interest to observe the enhancement of the absorption rate when the laser width is narrower than the atomic linewidth. The enhancement is expected to be a factor of three, due to the large intensity fluctuations of the field. The total bandwidth of the absorption line and its dependence on laser bandwidth will also be measured. Another experiment in the works is to measure the intensity fluctuations on the light transmitted by a Fabry-Pérot interferometer when excited by the real Gaussian field. Future plans also include extension of this technique to generating the thermal field.

In closing, we remark that this field has a resemblance to a squeezed optical state. One quadrature of the light field has a much larger uncertainty than the other. A very important distinction between the real Gaussian field (as we have generated it) and a squeezed field is that our field is not a minimum uncertainty state, and that the uncertainty of the small field quadrature component has not been reduced in any way. The other quadrature has simply been increased through the random modulation process.

ACKNOWLEDGMENTS

This work is supported by a grant from the Department of Energy, Office of Basic Energy Sciences. Technical assistance from M. Mohebbi and B. Ferguson is gratefully acknowledged.

[1]B. R. Mollow, Phys. Rev. **175**, 1555 (1968).
[2]S. N. Dixit, P. Zoller, and P. Lambropoulos, Phys. Rev. A **21**, 1289 (1980).
[3]K. Wódkiewicz and J. H. Eberly, Phys. Rev. A **31**, 2314 (1985).
[4]L. A. Lompré, G. Mainfray, C. Manus, and J. P. Mariner, J. Phys. B **14**, 4307 (1981).
[5]M. W. Hamilton, K. Arnett, S. J. Smith, D. S. Elliott, M. Dziemballa, and P. Zoller, Phys. Rev. A **87**, 178 (1987).
[6]R. Boscaino and R. N. Mantegna, Phys. Rev. A **40**, 5 (1989); *ibid.* **40**, 13 (1989).
[7]G. S. Agarwal, Phys. Rev. A **1**, 1445 (1970).
[8]R. Boscaino and R. N. Mantegna, Opt. Commun. **73**, 289 (1989).
[9]A. T. Georges, Phys. Rev. A **21**, 2034 (1980).
[10]D. S. Elliott, M. W. Hamilton, K. Arnett, and S. J. Smith, Phys. Rev. A **32**, 887 (1985); K. Arnett, S. J. Smith, R. E. Ryan, T. Bergeman, H. Metcalf, M. W. Hamilton, and J. R. Brandenberger, Phys. Rev. A **41**, 2580 (1990); M. W. Hamilton (unpublished).
[11]F. T. Arecchi, Phys. Rev. Lett. **15**, 912 (1965).
[12]Gautum Vemuri, Rajarshi Roy, and G. S. Agarwal, Phys. Rev. A **41**, 2749 (1990).
[13]G. S. Agarwal (private communication).
[14]C. E. Weiman and C. Tanner (private communication); L. Hollberg (private communication).
[15]Th. Haslwanter, H. Ritsch, J. Cooper, and P. Zoller, Phys. Rev. A **38**, 5652 (1988).
[16]M. H. Anderson, R. D. Jones, J. Cooper, S. J. Smith, D. S. Elliott, H. Ritsch, and P. Zoller, Phys. Rev. Lett. **64**, 1346 (1990).
[17]B. A. Ferguson and D. S. Elliott, Phys. Rev. A (to be published).
[18]D. S. Elliott and S. J. Smith, J. Opt. Soc. Am. B **5**, 1927 (1988).
[19]See, for example, A. Papoulis, *Probability, Random Variables and Stochastic Processes*, 2nd ed. (McGraw-Hill, New York, 1984), p. 265.